
This is an electronic reprint of the original article.
This reprint may differ from the original in pagination and typographic detail.

Dahal, Roshi; Uusi-Kyyny, Petri; Pokki, Juha Pekka; Alopaeus, Ville

Vapor- liquid equilibrium for the n-dodecane + phenol and n-hexadecane + phenol systems at 523 K and 573 K

Published in:
Fluid Phase Equilibria

DOI:
[10.1016/j.fluid.2021.112991](https://doi.org/10.1016/j.fluid.2021.112991)

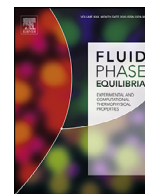
Published: 01/06/2021

Document Version
Publisher's PDF, also known as Version of record

Published under the following license:
CC BY

Please cite the original version:
Dahal, R., Uusi-Kyyny, P., Pokki, J. P., & Alopaeus, V. (2021). Vapor- liquid equilibrium for the n-dodecane + phenol and n-hexadecane + phenol systems at 523 K and 573 K. *Fluid Phase Equilibria*, 537, Article 112991. <https://doi.org/10.1016/j.fluid.2021.112991>

This material is protected by copyright and other intellectual property rights, and duplication or sale of all or part of any of the repository collections is not permitted, except that material may be duplicated by you for your research use or educational purposes in electronic or print form. You must obtain permission for any other use. Electronic or print copies may not be offered, whether for sale or otherwise to anyone who is not an authorised user.



Vapor- liquid equilibrium for the *n*-dodecane + phenol and *n*-hexadecane + phenol systems at 523 K and 573 K

Roshi Dahal^{a,*}, Petri Uusi-Kyyny^a, Juha-Pekka Pokki^a, Ville Alopaeus^{a,b}

^aAalto University, School of Chemical Engineering, Department of Chemical and Metallurgical Engineering, P.O. Box 11000, FI-00076 Aalto, Finland

^bMid Sweden University, Department of Chemical Engineering, Sundsvall, 85170, Sweden

ARTICLE INFO

Article history:

Received 6 October 2020

Revised 16 February 2021

Accepted 23 February 2021

Available online 3 March 2021

Keywords:

Bubble point method

Continuous flow apparatus

Dodecane

Hexadecane

Phenol

Modeling

ABSTRACT

A continuous flow apparatus was applied to measure the phase equilibrium at 523 K and 573 K. The performance of the apparatus was analysed with the determination of vapor pressures of water at the temperatures ($T = 453$ K and 473 K). The measured water vapor pressures deviated from the literature values less than 1 %. Vapor pressures of *n*-dodecane, *n*-hexadecane and phenol were measured at the temperatures ($T = 523$ – 623 K) and, the bubble point pressures of *n*-dodecane + phenol and *n*-hexadecane + phenol were measured at the temperatures ($T = 523$ K and 573 K). The measured vapor pressures of the pure components were compared with the literature values. Relative vapor pressure deviated from the literature value less than 2 % for all the measured vapor pressures. The measured vapor pressures value in this work agreed well with the literature, which indicates that the measurement apparatus and the method can produce good-quality data. The measured bubble point pressures for the *n*-dodecane + phenol and *n*-hexadecane + phenol systems were modeled with Peng-Robinson and Perturbed-Chain Statistical Associating Fluid Theory (PC-SAFT) equations of state and Non-random Two-liquid (NRTL) activity coefficient model. The measured systems were at first modeled with Peng-Robinson and Perturbed-Chain Statistical Associating Fluid Theory (PC-SAFT) equations of state without binary interaction parameters. Additionally, the parameters were regressed to optimize the performance of the models. The NRTL activity coefficient model described the behaviour of the measured and the literature data better than the equations of state. Furthermore, the Peng-Robinson equation of state resulted in better predictions than PC-SAFT equation of state even without binary interaction parameters regression. Both equations of state modeled the phase equilibrium behaviour of the system well. The *n*-dodecane + phenol system showed azeotropic behaviour.

© 2021 The Author(s). Published by Elsevier B.V.

This is an open access article under the CC BY license (<http://creativecommons.org/licenses/by/4.0/>)

1. Introduction

The increasing energy demand and negative environmental impacts due to the use of fossil fuels have directed modern society to search and adopt renewable and sustainable energy sources. The use of biomass as a renewable source and its energy conversion via fast pyrolysis has already undergone scale-up [1]. In recent days, chemical recycling of waste plastics via pyrolysis has been an interest of study [2,3]. The increasing production of plastics and low recycling rates have led to increment of plastic wastes [3], which shows that there is considerable scope of improvement. Traditionally produced from petroleum by-products, plastic polymers are rich in hydrocarbons [4]. Pyrolysis of plastics results in hydrocarbon rich oil with excellent fuel properties [5]. In addition,

co-pyrolysis of biomass and waste plastic could result efficient method to improve the oil fraction [6].

Pyrolysis oil is a liquid product derived from biomass or waste plastics or both pyrolysis, which could be further employed in various downstream applications subjected to appropriate upgrading and refining [1,3]. However, the complex mixture of pyrolysis oil consists of hundreds of oxygenated compounds [7], which is one of the major challenges in process design [8]. Therefore, there is a need for reliable and predictive thermodynamic models to reproduce the multiphase behaviour of the main components for the design of separation processes. On the other hand, due to lack of experimental data for such complex systems, the phase behaviour of pyrolysis oil compounds requires further study for the development of predictive models [8].

Within these contexts, this work outlines the phase equilibrium behaviour of selected model components of pyrolysis oil. Hydrocarbons are the basis for the production of fuel and chemicals. The platform chemicals present in bio-oil are often converted to

* Corresponding author.

E-mail address: roshi.dahal@aalto.fi (R. Dahal).

List of symbols

abs	absolute
A	parameter in the extended form of Antoine's equation
B	parameter in the extended form of Antoine's equation
C	parameter in the extended form of Antoine's equation
D	parameter in the extended form of Antoine's equation
E	parameter in the extended form of Antoine's equation
k	binary interaction parameter in the Peng-Robinson and PC-SAFT equation of states
m	segment number in the PC-SAFT equation of state
M	molar mass (g mol ⁻¹)
n	number of moles (mol)
N	number of data points
P	pressure (Pa)
Q	objective function in the regression
T	temperature (K)
v ₁	molar volume (cm ³ mol ⁻¹)
V	volumetric flow rate (cm ³ min ⁻¹)
w	mass (kg)
x	liquid mole fraction
z	total mass fraction

Greek letters

ϵ/k	segment energy parameter (K) in PC-SAFT equation of state
ϵ^{AiBi}/k	association energy parameter (K) in PC-SAFT equation of state
k^{AiBi}	effective association volume in PC-SAFT equation of state
σ	segment diameter (Å) in PC-SAFT equation of state
ρ	density (kg m ⁻³)

Subscripts

A	absolute
AVG	average deviation
C	critical property
calc	calculated
i	component i
j	component j
lit	literature
meas	measured
R	relative

hydrocarbons via hydrodeoxygenation to produce renewable fuel and chemicals [9]. Similarly, the pyrolysis of polyalkene plastics like polyethylene (PE) and polypropylene (PP) yields oils and waxes with mainly aliphatic composition consisting of a series of alkanes, alkenes and alkadienes [10,11]. Thus, the derived oils and waxes show great potential as a feedstock for the production of new plastics or refined fuels. Alkanes such as *n*-dodecane and *n*-hexadecane exhibit excellent solvent properties and are applied for the fuel production as well.

In this work, bubble point pressures for the mixtures of *n*-dodecane + phenol and *n*-hexadecane + phenol have been measured at 523.15 K and 573.15 K. The measurements were conducted using high-pressure apparatus with the continuous flow bubble point detection method. The phase transition was observed with a video camera integrated within the measurement apparatus. The bubble point pressures of water were measured to demonstrate the

performance of the apparatus and the measuring method. Isothermal vapor-liquid equilibria of *n*-dodecane + phenol have been measured by Schmelzer et al. [31] 393.15 K and 433.15 K and isobaric vapor-liquid equilibria of *n*-dodecane + phenol at 101.32 kPa have been presented by Aarna et al. [32]. No phase equilibrium data were found for *n*-hexadecane + phenol system in the literature. The measured systems were modeled with Peng-Robinson [12] and Perturbed-Chain Statistical Associating Fluid Theory (PC-SAFT) [13] equations of state and Non-random Two-liquid (NRTL) activity coefficient model [14].

2. Experimental**2.1. Materials**

Table 1 lists the materials and their specifications. Milli-Q ultrapure water (Type I) was obtained from the water purification system (Direct-Q 5 UV).

2.2. Apparatus

The sapphire tube-equipped continuous flow apparatus was adopted for the determination of pure component vapor pressures and bubble point pressures of mixtures. Uusi-Kyyny et al. [15] detail the construction and operation of the equipment. In this work, the equipment was operated with slight modifications. The experimental set-up is presented in Fig. 1. The apparatus consisted of three syringe pumps, two separate pumps for pumping fluid to the system (Isco Teledyne, model 260D) and one for receiving the fluid (Isco Teledyne, model 500D), a high-pressure micro mixer (micro4industries GmbH, Germany), an oven taken from an old gas chromatograph (HP 5890 Series II), electrically traced lines and the equilibrium cell (maximum allowed conditions <673 K and <20 MPa). The equilibrium cell consisted of sapphire glass windows with a temperature probe integrated into the cell. The temperature of the pumps was controlled with a circulator thermostat. The temperature control of the pumps and the electrical tracing of the lines was required to prevent phenol solidification (melting point of phenol 314.06 K [16]) and cloggage in the lines at room temperature. The temperature control unit (Meyer-vastus) equipped with a sensor (Pt-100) was used for controlling the temperature of the heat tracing. The two feed lines were connected to the micro mixer to mix the components before being fed into the cell. For the mixtures prepared gravimetrically, only one feed pump (Isco Teledyne, model 260D) was used. A video camera was employed to record the phase change of the fluid in the equilibrium cell through the oven windows. The lines were constructed of stainless-steel narrow tubes (AISI 316) with an internal diameter of 1 mm. Cell temperature and pressure were continuously logged using Keysight 34972a Digital Multimeter.

Temperatures were measured with Pt-100 probes. The probes were calibrated against the Tempcontrol CTR-2000-24 thermometer equipped with a reference Pt-100 probe, which was calibrated at the Finnish National Standards Laboratory (MIKES). The expanded uncertainty of the digital thermometer was estimated to be ± 0.12 K (with the coverage factor $k = 2$). The equilibrium cell temperature was measured with a temperature probe inserted inside the cell through a T-piece. The temperatures of the syringe pumps were measured with the temperature probes (the Tempcontrol CTR-2000-24 thermometer equipped with Pt-100 probes) placed in contact with the syringe pump barrels.

The pressure was measured in the line between the equilibrium cell and the receiving pump with a (absolute) pressure transducer (type GE UNIK, pressure range 0–10 MPa, uncertainty for pressure measurement 0.0004 MPa using a coverage factor $k=2$) at room

Table 1
Lists of chemicals with their specifications.

Component	CAS number	Supplier	Purity ^a , mass fraction	Purification method
Phenol	108-95-2	Sigma-Aldrich	≥ 0.99	None
<i>n</i> -dodecane	112-40-3	Merck KGaA	≥ 0.99	None
<i>n</i> -hexadecane	544-76-3	Sigma-Aldrich	≥ 0.99	None
		Merck KGaA	≥ 0.99	None
Water	–	Aalto University	Not determined	Ultra-purification

^a The purity as reported by the supplier.

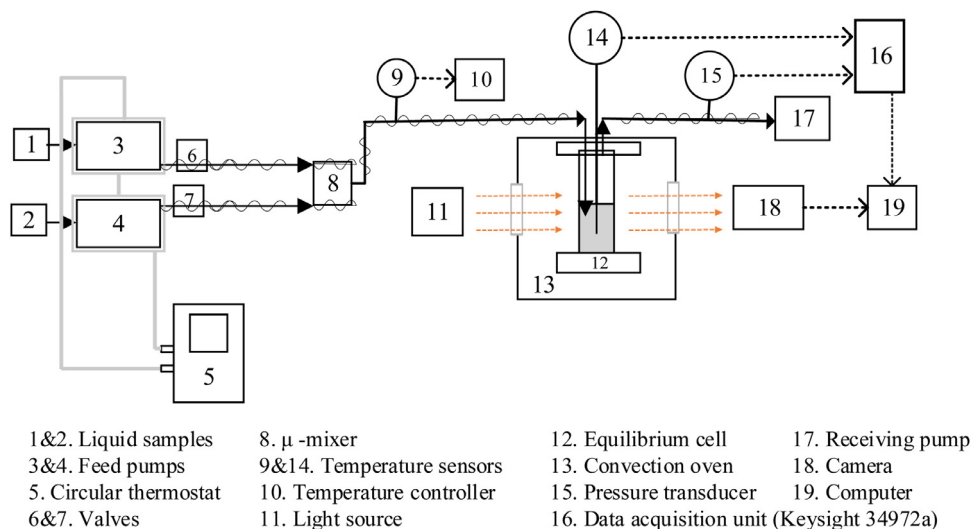


Fig. 1. Schematic figure of continuous flow apparatus. Tubing (black solid arrows); electrical signals (black dashed arrows); light (orange dashed arrows); water pipelines (solid grey lines); heat trace (zigzag lines around the tubing, μ -mixer and valves).

temperature. The measured pressure was recorded from the multimeter (type Keysight 34972a, output range 4–20 mA, uncertainty for pressure measurement 0.00035 using coverage factor $k=2$). The pressure sensor was calibrated against a Beamex MC2-PE calibrator equipped with an external pressure module: EXT60 (pressure calibration uncertainty 0.0031 MPa, using coverage factor $k=2$). The calibrator is periodically calibrated at Beamex Oy, Finland. The expanded uncertainty corresponding to pressure measurements was estimated to be 0.0032 MPa. The pressures of the syringe pump barrels were controlled with built-in strain gauge pressure meters in the pumps. Furthermore, the apparatus performance was evaluated with the determination of vapor pressure of water. The vapor pressures were in agreement with the literature value presented in Table 5.

2.3. Procedure

The bubble point measurement procedure was conducted with an approach similar to earlier work [15]. The developed measurement scheme was based on continuous fluid flow through the apparatus. The apparatus operation begun with constant flow rate at a pressure higher than the bubble point pressure. The pressure was decreased at a controlled rate until the bubble point was observed. The phase transition in the equilibrium cell was visually observed.

The lines and the feed pumps (Isco pump 1 and 2) were evacuated using a vacuum pump prior to feeding the degassed liquid samples. Prior to the measurements, the flow and temperature in the apparatus were let to stabilize. The flow rates from the feed pumps were calculated and set to achieve the targeted mixture compositions in the equilibrium cell. The sample was pumped through the apparatus at a continuous flow rate to the measurement pump (Isco pump 3). Afterwards, the measurement pump

was set to the initial pressure of measurement. The time needed for stabilizing the flow before the first measurement and after each temperature change was about 45 min.

2.4. Uncertainty estimation

The extended experimental uncertainties U is calculated using Equation (1),

$$U = (kU_c) = k\sqrt{\sum (U_i)^2} \quad (1)$$

where U_i is the standard uncertainty of each influencing component, U_c is the combined standard uncertainty of each influencing element, and k is the confidence interval [17]. In this work, the coverage factor $k = 2$, which corresponds to a 95 % degree of confidence, is applied to characterize the measurements. Table 2 presents the standard uncertainties of the influencing components. For the vapor pressure measurements, the main uncertainty arises from the thermometers and pressure meters. For the bubble point pressure measurements, the pump set-point resolution is the main uncertainty factor.

The uncertainties of temperature, pressure, density correlation, pump flow rate and balance were taken into consideration for the determination of the uncertainty in the mole fraction. The mixtures with lower phenol concentration ($x_{phenol} < 0.1$) were gravimetrically prepared using a balance (Precisa, XT 620M). The values of the individual uncertainties are given in Table 3.

To estimate the uncertainty on the overall composition of the mixture pumped through the cell, the uncertainty in the number of moles is derived. By differentiating the injected amount of moles n_1 we obtain,

$$dn_1 = d\left(\frac{\rho_1(T, p) V_1}{M_1}\right) \quad (2)$$

Table 2

Uncertainty components (with their standard uncertainties) of the vapor pressure and the bubble point pressure measurements.

Vapor Pressure Measurement	
u_{pressure} (MPa)	
pressure calibration uncertainty	0.00156
pressure sensor uncertainty, by manufacturer	0.0002
display unit 34091A multiplexer unit, by manufacturer	0.000175
combined uncertainty, $u_{c,\text{pressure}}$	0.0016
$u_{\text{temperature}}$ (K)	
temperature measurement device uncertainty	0.03
temperature calibration uncertainty	0.05
combined uncertainty, $u_{c,\text{temperature}}$	0.06
Bubble Point Measurement	
u_{pressure} (MPa)	
set-point resolution of the pump	0.005
pressure calibration uncertainty	0.00156
pressure sensor uncertainty, by manufacturer	0.0002
display unit 34091A multiplexer unit, by manufacturer	0.000175
combined uncertainty, $u_{c,\text{pressure}}$	0.005
$u_{\text{temperature}}$ (K)	
temperature measurement device uncertainty	0.03
temperature calibration uncertainty	0.05
combined uncertainty, $u_{c,\text{temperature}}$	0.06

Table 3

Individual uncertainties employed for the estimation of uncertainty in mole fraction.

Influencing component	Uncertainty
Pressure, Bubble point pressure measurements	0.01 MPa
Pressure, Vapor pressure measurements	0.0032 MPa
Temperature	0.12 K
DIPPR density correlation uncertainty for phenol, <i>n</i> -dodecane and <i>n</i> -hexadecane [16]	$\pm 0.01\rho$
Set-point accuracy of the pumps; V = flow rate (cm ³)	0.5 % of V
Balance	0.006 g

which results as an equation for the theoretical standard uncertainty,

$$\Delta n_1 = \frac{V_1}{M_1} \Delta \rho_1 + \frac{V_1}{M_1} \left(\left| \frac{d\rho_1}{dT} \right| \Delta T + \frac{d\rho_1}{dp} \Delta p \right) + \frac{\rho_1}{M_1} \Delta V_1 \quad (3)$$

The modification of the pressure derivative of density gives,

$$\Delta n_1 = \frac{V_1}{M_1} \Delta \rho_1 + \frac{V_1}{M_1} \left(\left| \frac{d\rho_1}{dT} \right| \Delta T + \left(-\frac{m_1}{V_1^2} \frac{dV_1}{dp} \Delta p \right) \right) + \frac{\rho_1}{M_1} \Delta V_1 \quad (4)$$

By taking $\rho_1 V_1 / M_1 = n_1$ as a multiplier,

$$\Delta n_1 = n_1 \left(\frac{\Delta \rho_1}{\rho_1} + \frac{1}{\rho_1} \left| \frac{d\rho_1}{dT} \right| \Delta T + \left(-\frac{1}{V_1} \left(\frac{dV_1}{dp} \right)_T \right) \Delta p + \frac{\Delta V_1}{V_1} \right) \quad (5)$$

and setting κ_1 which is the isothermal compressibility given as,

$$\kappa_1 = -\frac{1}{V_1} \left(\frac{dV_1}{dp} \right)_T \quad (6)$$

Replacing κ_1 in Equation (5), we obtain,

$$\Delta n_1 = n_1 \left(\frac{\Delta \rho_1}{\rho_1} + \frac{1}{\rho_1} \left| \frac{d\rho_1}{dT} \right| \Delta T + \kappa_1 * \Delta p + \frac{\Delta V_1}{V_1} \right) \quad (7)$$

The corresponding equation is also valid for Component 2. In Equation (7) temperature derivative of density was calculated from the density correlation [18] and the compressibility of a liquid was obtained from the Hankinson–Brobst–Thompson model [19]. Thus,

the uncertainty estimate in overall mole fractions was determined from,

$$\Delta z_1 = \left| \frac{n_1}{(n_1 + n_2)} - \frac{(n_1 + \Delta n_1)}{(n_1 + \Delta n_1) + (n_2 - \Delta n_2)} \right| \quad (8)$$

The uncertainty determination for the gravimetric mixtures is presented in Equation (9), here the uncertainty of the scale (Δw) was taken in account. The uncertainty estimate in overall mole fractions was determined using,

$$\Delta z_1 = \left(\left| \frac{\Delta w_1}{w_1} \right| + \left| \frac{\frac{\Delta w_1}{M_1}}{\frac{w_1}{M_1} + \frac{w_2}{M_2}} \right| + \left| \frac{\frac{\Delta w_2}{M_2}}{\frac{w_1}{M_1} + \frac{w_2}{M_2}} \right| \right) z_1 \quad (9)$$

3. Results

3.1. Vapor pressures of pure components

Vapor pressures of pure components phenol, water, *n*-hexadecane and dodecane were measured with the continuous flow apparatus. The measured vapor pressures of phenol, *n*-hexadecane and *n*-dodecane were compared with the values calculated from the DIPPR 101 equation [16],

$$P_i/\text{Pa} = \exp(A + B/(T/K) + C \ln(T/K) + D(T/K)^E) \quad (10)$$

where P_i is the vapor pressure in Pascal (Pa) of the pure component i at the system temperature T in Kelvin unit (K). Table 4 lists the parameters A through E obtained from the literature [16].

The DIPPR vapor pressure correlation uncertainty for phenol is given as 3 % [16]. The DIPPR uncertainty designations are approximate and the DIPPR uncertainty will rarely be the same as experimental estimates [20]. It was observed that the calculated vapor pressures of phenol using correlation deviated from the experimental vapor pressures at 523K and 573 K with 2.5 %. However, this deviation was higher than the experimental uncertainty (in Table 2). Therefore, the vapor pressure correlation parameters for phenol were regressed. The regression was performed using the vapor pressure data from this work ($T = 523$ K and 573 K) and the literature data ($T = 393$ K and 433 K) [31] in order to correlate the measured and the calculated vapor pressures for elevated temperatures. The experimental vapor pressure of phenol deviated from the calculated vapor pressure using new regressed parameters with 1.6 %, in Table 5. Further, the calculated vapor pressures of *n*-alkanes using the correlation were in-line with the measured vapor pressures, thus the DIPPR correlation parameters were employed for *n*-dodecane and *n*-hexadecane.

The measured vapor pressures of water were compared with the reference values [21].

The measured and calculated vapor pressure values for all components are presented in Table 5 and compared in Fig. 2. The absolute and relative average vapor pressure deviations were calculated to evaluate the agreement between the measured vapor pressures and values calculated with the literature correlation. These deviations for water, phenol, *n*-hexadecane and *n*-dodecane are presented in Table 5. The deviations are within the uncertainty of correlation used and the experimental uncertainty. It indicates the measured vapor pressures values agree well with the calculated ones. In addition, the performance of the apparatus and the measurement method was proven reliable.

3.2. Bubble point pressures measurements and modeling

The bubble point pressures for the systems of *n*-dodecane + phenol and *n*-hexadecane + phenol were measured with a continuous flow apparatus under isothermal conditions. The

Table 4
Parameters for pure components used in calculations.

	Phenol	n-hexadecane	n-dodecane	Water
MW^a /g mol ⁻¹	94.1112	226.441	170.335	18.0153
T_c^b /K	694.25	723	658	647.10
P_c^c /MPa	6.13	1.4	1.82	22.06
v_l^d /m ³ kmol ⁻¹	0.0889403	0.294213	0.228605	0.0180691
ω^e	0.44346	0.717404	0.576385	0.344861
A^f	61.9874*	156.06	137.47	73.649
B^f	-8135.75*	-15015	-11976	-7258.2
C^f	-5.3197*	18.941	-16.698	-7.3037
D^f	0	6.8172E-06	8.0906E-06	4.1653E-06
E^f	0	2	2	2
T_{min}^f /K	393.15	291.30	263.57	273.16
T_{max}^f /K	573.15	723	658	647.09
m_i^g	3.78605	6.6485	5.3060	1.0656
σ_i^g /Å	3.2007	3.9552	3.8959	3.0007
ϵ_i/k^g /K	293.649	254.70	249.21	366.51
$k^{AIBI, g}$	0.00634	-	-	0.034868
ϵ^{AIBI}/k^g /K	1640.63	-	-	2500.7
$\Delta P_{vap,A,AVG}^h$ /MPa	0.001	0.0004	0.0005	-
$\Delta v_{i,A,AVG}^i$ /cm ³ mol ⁻¹	0.53	2.0	1.7	-
T_{range}^j /K	343–585	314–625	263–573	-

^a Ref. [16] Molecular weight, MW .

^b Ref. [16] Critical pressure, T_c .

^c Ref. [16] Critical pressure, P_c .

^d Ref. [16] Liquid molar volume at 298 K, v_l .

^e Ref. [16] Acentric factor, ω .

^f Ref. [16] Vapor pressure correlation parameters for the temperature range from T_{min} to T_{max} .

^g Ref. [21,22,34] PC-SAFT parameters: the segment number m_i , the segment diameter σ_i , the segment energy ϵ_i/k , the effective association volume k^{AIBI} , the association energy ϵ^{AIBI}/k .

^h Pure component average absolute vapor pressure deviation using PC-SAFT parameters: $\Delta P_{vap,A,AVG} = \frac{(\sum_{i=1}^N |P_{i,lit} - P_{i,calc}|)}{N}$ where N is the number of data points, $P_{i,lit}$ is the vapor pressure (Pa) value from the literature, $P_{i,calc}$ is the calculated vapor pressure (Pa).

ⁱ Pure component average absolute molar volume deviation using PC-SAFT parameters: $\Delta v_{i,A,AVG} = \frac{(\sum_{i=1}^N |v_{i,lit} - v_{i,calc}|)}{N}$ where N is the number of data points, $v_{i,lit}$ is the molar volume (cm³ mol⁻¹) value from the literature, $v_{i,calc}$ is the calculated molar volume (cm³ mol⁻¹).

^j Temperature range that was used in the regression of PC-SAFT parameters.

* The regressed vapor pressure correlation parameters of phenol using the measured vapor pressures in this work and the vapor pressures from the literature [31].

Table 5

Vapor pressures of water, phenol, n-hexadecane and n-dodecane from this work (P_{meas}), literature correlation (P_{lit}), pressure deviation (ΔP) and relative vapor pressure deviation ($P_{vap,R}$) at temperature (T).

Component	T /K	P_{meas} /MPa	P_{lit}^a /MPa	ΔP^b /MPa	$P_{vap,R}^c$ /%
Water	453.6	1.006	1.004 ^d	0.002	0.20
	473.4	1.565	1.562 ^d	0.003	0.19
Phenol	524.4	0.491	0.499	-0.008	1.63
	574.8	1.206	1.194	0.012	1.00
n-hexadecane	523.7	0.043	0.043	0.00	0
	574.1	0.137	0.137	0.00	0
n-dodecane	523.4	0.213	0.213	0.00	0
	573.1	0.530	0.530	0.00	0
	623.1	1.151	1.138	0.013	1.13

The extended uncertainties of temperature and pressure were calculated using a coverage factor $k = 2$, $u(T) = 0.12$ K and $u(P) = 0.0032$ MPa.

Vapor pressure correlation uncertainty was given 3 % [16].

Vapor pressure uncertainty of water for the literature value was given 0.05 % [21].

^a The values are calculated from Equation (10).

^b Pressure deviation, $\Delta P = P_{meas} - P_{lit}$

^c Relative vapor pressure deviation $P_{vap,R} = |(P_{i,meas} - P_{i,lit})/P_{i,meas}|$ where $P_{i,meas}$ is the measured vapor pressure, $P_{i,lit}$ is the calculated vapor pressure from correlation [16].

^d Values from the reference [21].

results from the bubble point measurements of *n*-dodecane + phenol and *n*-hexadecane + phenol are presented in Tables 6 and 7 respectively.

The *n*-dodecane + phenol and *n*-hexadecane + phenol systems were modeled with PC-SAFT [13,21] and Peng-Robinson equations

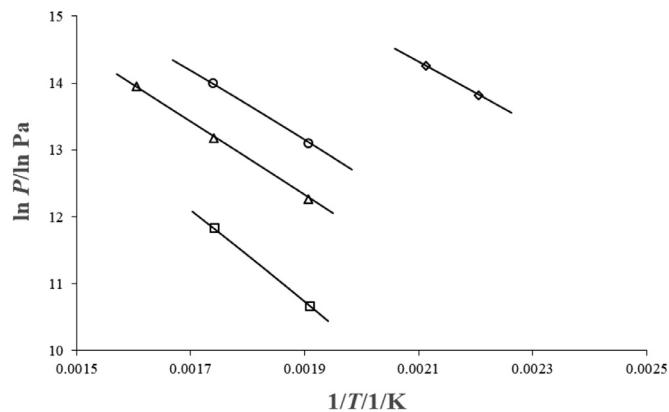


Fig. 2. Vapor pressures measured in this work for phenol (\circ), *n*-dodecane (Δ) and *n*-hexadecane (\square) and, compared with the values calculated using DIPPR 101 equation (—) at temperature (T). Measured vapor pressures of water (\diamond) are compared with the reference value [21].

of state [12] and, NRTL activity coefficient model [14]. The measured data were processed with Aspen Plus (V11). The regression was performed with method similar to previous work [24]. The PC-SAFT and Peng-Robinson equations of state were applied in two modes. In the first mode, the models were employed without the regression of the binary interaction parameters in a predictive mode. In the second mode, the binary interaction parameters were

Table 6

Measured bubble point pressures (P) for temperature (T), phenol mole fraction (z) with uncertainty ($u(z_{phenol})$) for the system n -dodecane + phenol.

T/K	P/MPa	z_{phenol}	$u(z_{phenol})$	T/K	P/MPa	z_{phenol}	$u(z_{phenol})$
523.4	0.213	0.000	0	573.1	0.530	0.000	0
523.6	0.216	0.021 ^x	0.0001	574.6	0.579	0.021 ^x	0.0001
524.5	0.272	0.051 ^x	0.0001	574.7	0.646	0.051 ^x	0.0001
524.2	0.288	0.069 ^x	0.0001	574.7	0.682	0.069 ^x	0.0001
523.9	0.301	0.101	0.003	574.8	0.754	0.101	0.003
524.2	0.361	0.201	0.005	575.0	0.866	0.201	0.005
524.3	0.419	0.301	0.006	574.8	0.951	0.301	0.006
524.4	0.448	0.401	0.007	575.1	1.036	0.401	0.007
524.5	0.474	0.502	0.008	575.2	1.123	0.502	0.008
523.2	0.496	0.601	0.007	574.9	1.177	0.601	0.007
524.4	0.515	0.701	0.006	574.7	1.215	0.701	0.006
524.6	0.523	0.801	0.005	574.7	1.236	0.801	0.005
524.7	0.521	0.901	0.003	574.7	1.249	0.901	0.003
524.4	0.491	1.000	0	574.8	1.206	1.000	0

The extended uncertainties of temperature and pressure were calculated using a coverage factor $k = 2$, $u(T) = 0.12$ K and $u(P) = 0.01$ MPa. The uncertainties in compositions were calculated from total derivative using equations 8 and 9. The bubble point pressures are provided with 3 decimal digits to reduce error in subsequent analysis.

^x mixtures prepared gravimetrically.

Table 7

Measured bubble point pressures (P) for temperature (T), phenol mole fraction (z) with uncertainty ($u(z_{phenol})$) for the system n -hexadecane + phenol.

T/K	P/MPa	z_{phenol}	$u(z_{phenol})$	T/K	P/MPa	z_{phenol}	$u(z_{phenol})$
523.7	0.043	0.000	0	574.1	0.137	0.000	0
524.7	0.059	0.021 ^x	0.0001	575.1	0.191	0.021 ^x	0.0001
524.8	0.084	0.039 ^x	0.0001	575.0	0.203	0.039 ^x	0.0001
525.1	0.099	0.059 ^x	0.0001	575.2	0.235	0.059 ^x	0.0001
524.0	0.130	0.100	0.003	574.1	0.335	0.100	0.003
524.0	0.196	0.200	0.005	574.9	0.464	0.200	0.005
524.4	0.272	0.301	0.006	574.9	0.595	0.301	0.006
523.8	0.302	0.401	0.007	574.8	0.720	0.401	0.007
524.0	0.343	0.489	0.008	574.8	0.813	0.489	0.008
524.0	0.380	0.593	0.007	574.7	0.887	0.593	0.007
524.3	0.416	0.694	0.006	574.8	0.988	0.694	0.006
524.6	0.447	0.800	0.005	574.8	1.057	0.800	0.005
524.3	0.466	0.898	0.003	574.7	1.154	0.898	0.003
524.4	0.491	1.000	0	574.8	1.206	1.000	0

The extended uncertainties of temperature and pressure were calculated using a coverage factor $k = 2$, $u(T) = 0.12$ K and $u(P) = 0.01$ MPa. The uncertainties in compositions were calculated from total derivative using equations 8 and 9. The bubble point pressures are provided with 3 decimal digits to reduce error in subsequent analysis.

^x mixtures prepared gravimetrically.

regressed against the experimental data. The NRTL activity coefficient model was applied only in the second mode for parameters regression.

The maximum likelihood objective function (Q), which is the generalization of the least-squares method [25], was used for the bubble point regression in Equation (11). The equation takes into account all the measured T , P , x and y values. In this work, the vapor mole fraction (y) was not measured, therefore y is excluded during the calculation. On the other hand, the literature data [31] includes both x and y values and these values were employed in the regression. Therefore, the general form of maximum likelihood equation is presented in Equation (11).

$$Q = \sum_{n=1}^{NDG} w_n \sum_{i=1}^{NP} \left[\left(\frac{T_{e,i} - T_{m,i}}{\sigma_{T,i}} \right)^2 + \left(\frac{P_{e,i} - P_{m,i}}{\sigma_{P,i}} \right)^2 \right] + \sum_{j=1}^{NC-1} \left(\frac{x_{e,i,j} - x_{m,i,j}}{\sigma_{x,i,j}} \right)^2 + \sum_{j=1}^{NC-1} \left(\frac{y_{e,i,j} - y_{m,i,j}}{\sigma_{y,i,j}} \right)^2 \quad (11)$$

where:

Q	The objective function to be minimized by data regression
NDG	The number of data groups in the regression case
w_n	The weight of data group n
NP	The number of points in data group n
NC	The number of components present in the data group
T, P, x, y	Temperature, pressure, liquid and vapor mole fractions
E	Estimated data
M	Measured data
I	Data for data point i
J	Fraction data for component j
Σ	Standard deviation of the indicated data

3.2.1. Peng-Robinson equation of state

The Peng–Robinson equation of state requires three parameters for each component: critical temperature (T_c), critical pressure (P_c) and acentric factor (ω) [12]. For calculating the properties of mixtures, a mixing rule is required. This work applies the Peng–Robinson equation of state with 1) the standard quadratic mixing rule for attractive term with a temperature-independent binary interaction parameter (k_{ij}) and 2) the linear mixing rule for the co-volume term to calculate the properties of multicomponent sys-

Table 8

The binary interaction parameters of the Peng-Robinson (k_{ij}) and the PC-SAFT (k_{ij}) equations of states, the absolute ($\Delta P_{A,AVG}/\text{MPa}$) and relative ($\Delta P_{R,AVG}/\text{MPa}$) average pressure deviations for *n*-dodecane + phenol and *n*-hexadecane + phenol systems.

Model	System					
	<i>n</i> -dodecane + phenol			<i>n</i> -hexadecane + phenol		
	k_{ij}	$\Delta P_{A,AVG}^a/\text{MPa}$	$\Delta P_{R,AVG}^b/\%$	k_{ij}	$\Delta P_{A,AVG}^a/\text{MPa}$	$\Delta P_{R,AVG}^b/\%$
PR	0	0.03 ^c	5.2 ^c	0	0.04 ^c	8.8 ^c
	-0.029	0.03 ^c	5.1 ^c	-0.032	0.04 ^c	8.6 ^c
	0	0.0023 ^d	8.3 ^d	-	-	-
	-0.029	0.0019 ^d	7.2 ^d	-	-	-
PC-SAFT	0	0.102 ^c	14.75 ^c	0	0.09 ^c	22.06 ^c
	0.039	0.03 ^c	5.3 ^c	0.057	0.02 ^c	6.38 ^c
	0	0.007 ^d	22.5 ^d	-	-	-
	0.039	0.002 ^d	6.3 ^d	-	-	-

^a The average absolute pressure deviation $P_{A,AVG} = \frac{(\sum_{i=1}^N |P_{i,meas} - P_{i,calc}|)}{N}$ where N is the number of data points, $P_{i,meas}$ is the measured pressure, $P_{i,calc}$ is the calculated pressure.

^b The relative average pressure deviation $P_{R,AVG} = \frac{(\sum_{i=1}^N |(P_{i,meas} - P_{i,calc})/P_{i,meas}|)}{N}$ where N is the number of data points $P_{i,meas}$ is the measured pressure, $P_{i,calc}$ is the calculated pressure.

^c Values measured in this work.

^d Literature data [31].

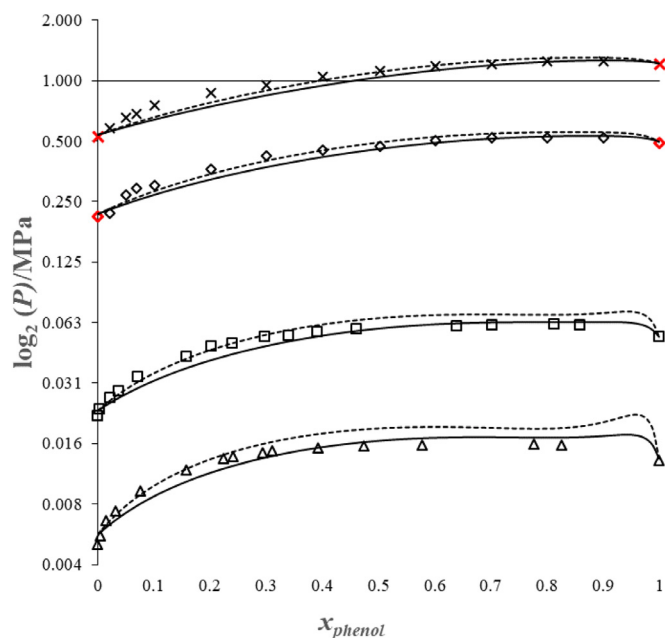


Fig. 3. The bubble point pressures (P) of *n*-dodecane + phenol system (x_{phenol} – mole fraction of phenol) measured in this work: (\diamond) 523 K, (\times) 573 K. Literature values [31]: (Δ) 393.15 K, (\square) 433.15 K. Calculated values with the Peng-Robinson equation of state: (.....) $k_{ij} = 0$, (–) $k_{ij} = -0.029$. Pure component vapor pressures measured in this work marked red.

tems. The parameters for the pure components are presented in Table 4.

The measured and modeled bubble point pressures of *n*-dodecane + phenol are shown in Fig. 3. The vapor-liquid equilibrium data for *n*-dodecane + phenol were obtained from the literature [31] at the temperature range 393.15–433.15 K. The binary interaction parameter was obtained from the regression of experimental data from this work and the literature data [31]. The absolute and relative pressure deviations were calculated for all predicted and optimized cases. The absolute and relative pressure deviations and the regressed binary interaction parameters are presented in Table 8. The behaviour of the measurements of this work are described adequately, even though the binary interaction parameter was regressed against the literature data points. From Table 8, small change in absolute and relative deviations were ob-

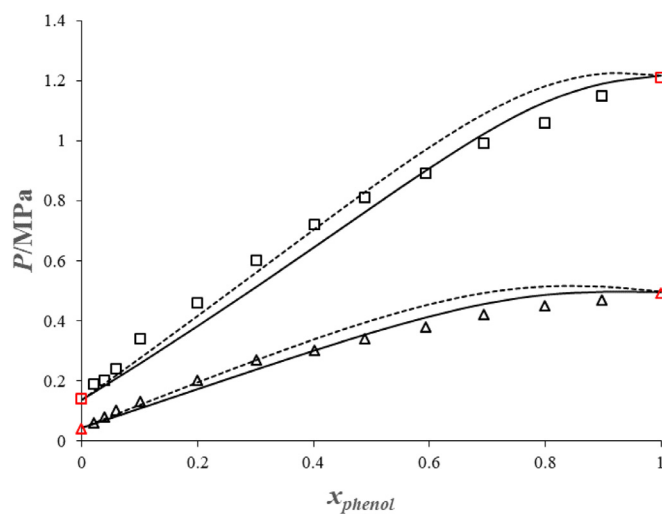


Fig. 4. The bubble point pressures (P) of *n*-hexadecane + phenol system (x_{phenol} – mole fraction of phenol) measured in this work: (Δ) 523 K, (\square) 573 K. Calculated values with the Peng-Robinson equation of state: (.....) $k_{ij} = 0$, (–) $k_{ij} = -0.032$. Pure component vapor pressures measured in this work marked red.

served with the parameter regression. Nevertheless, the ability of the model to predict the behaviour of the measurements without any parameter fit is also within an acceptable level.

It can be observed from Fig. 3 that the Peng-Robinson model without interaction parameters predicts a liquid-liquid split at the lower temperatures 393 K and 433 K [31]. After fitting the binary interaction parameter, the phase split reduces but does not disappear. The system is highly non-ideal which could possibly cause such behaviour with quadratic mixing rule in equation of state models. In addition, the PR binary parameters were optimized for each isothermal data separately. A plot was obtained employing the optimized binary parameters as a function of temperature which showed a linear trend with $R^2 = 0.9931$. The temperature dependent form of interaction parameter is expressed as $k_{ij} = 0.00012 * T/K - 0.081$. However, the model prediction was not notably improved on applying the temperature-dependent parameters.

The measured and modeled bubble point pressures of the *n*-hexadecane + phenol are shown in Fig. 4. The published data prior to this work were not found for the comparison. The absolute and relative pressure deviations and the regressed binary interaction

parameters are presented in Table 8. Fig. 4 shows that good agreement was achieved between the predictive results and the experimental data.

3.2.2. PC-SAFT equation of state

The PC-SAFT equation of state requires three basic pure-component parameters and in addition two association parameters if a component has tendency to associate. This associating interaction is considered by an association model proposed by Chapman et al. [26] based on Wertheim's first-order thermodynamic perturbation theory. Thus, an associating component is characterized by five pure-component parameters. The three basic parameters are the segment number (m_i), the segment diameter (σ_i) and the segment energy (ε_i/k) [22]. The association parameters are the effective association volume (k^{AiBi}) and the association energy (ε^{AiBi}/k) [13]. For predicting properties of mixtures, van der Waals one-fluid mixing rules and conventional Berthelot-Lorentz combining rules were applied with one binary interaction parameter k_{ij} [22].

The components *n*-dodecane and *n*-hexadecane are non-associating, whereas phenol is an associating component [27]. Huang and Radosz [27] described about the types of bonding in associating fluids such as water, alkanols, acid and amines. Each hydroxylic group (OH) in alkanols has association sites and association models are proposed based on the association sites. 2B and 3B association models are proposed for phenol (alkanols), where 2B is considered as assigned type (with 2 association sites) and 3B as rigorous type (with 3 association sites) [27]. In addition, Gross and Sadowski [13] outlined that all associating components are assigned two association sites; also referred as 2B model. Recently, NguyenHuynh et al. [8] described phenol by four parameter sets with different association schemes in addition of a dipolar term. The association scheme of phenol is complex to detail; however, association schemes are equally important for modeling. In this work, phenol is modeled as associating component with two association sites i.e. 2B association scheme.

The PC-SAFT parameters for phenol available in Aspen Plus and for hydrocarbons from literature [22] were adopted. These pure-component PC-SAFT parameters were evaluated against the pure component vapor pressure and the molar volume data retrieved with Aspen Plus from the NIST ThermoData Engine database. The absolute average vapor pressure and the molar volume deviations from the regression are presented in Table 4. The deviations were minimal and thus, the regression could be considered successful.

The measured and modeled bubble point pressures of *n*-dodecane + phenol are shown in Fig. 5. The vapor-liquid equilibrium data for the phenol *n*-dodecane + phenol were obtained from the literature [31] at the temperature range 393.15–433.15 K. The binary interaction parameter was obtained from the regression of experimental data in this work and the literature data [31]. The absolute and relative pressure deviations were calculated for predicted and optimized cases. The absolute and relative pressure deviations and, the regressed binary interaction parameters are presented in Table 8.

PC-SAFT prediction considerably improved when optimizing the temperature-independent binary interaction parameter regression in comparison to the predictive approach where the parameter was set to 0. The binary interaction parameter was regressed with the experimental data in this work and the literature data [31]. Fig. 5 shows that the experimental data fit against the regressed model is much better than the predictive one. This was also proven from the decreased average absolute and relative deviations with the binary interaction parameter regression in Table 8.

The measured and modeled bubble point pressures of *n*-hexadecane + phenol are presented in Fig. 6. Literature data prior to this work were not found for comparison. Fig. 6 indicates a clear improvement of the experimental data fit with the regressed

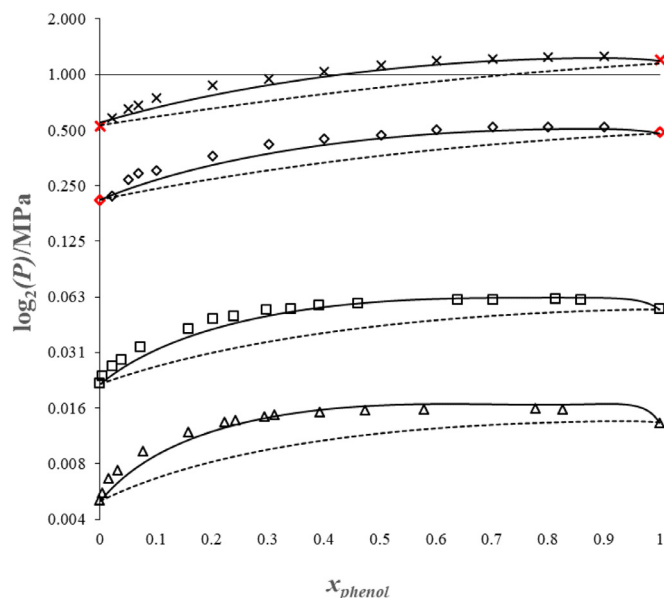


Fig. 5. The bubble point pressures (P) of *n*-dodecane + phenol system (x_{phenol} – mole fraction of phenol) measured in this work: (\diamond) 523 K, (\times) 573 K. Literature values [31]: (Δ) 393.15 K, (\square) 433.15 K. Calculated values with the PC-SAFT equation of state: (.....) $k_{ij} = 0$, (–) $k_{ij} = 0.039$. Pure component vapor pressures measured in this work marked red.

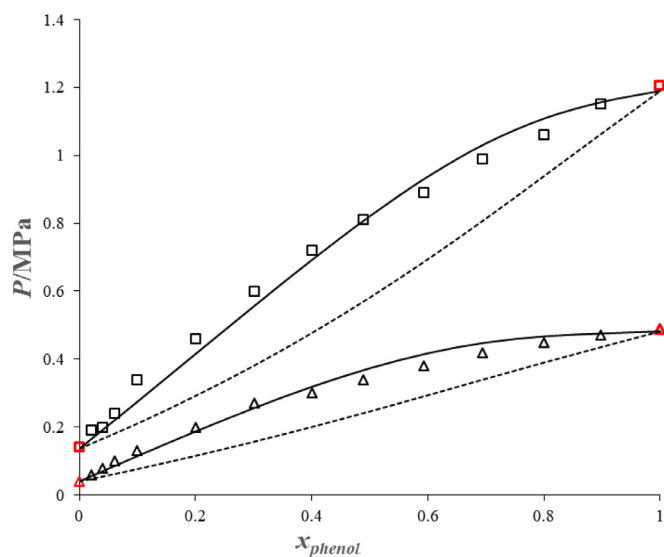


Fig. 6. The bubble point pressures (P) of *n*-hexadecane + phenol system (x_{phenol} – mole fraction of phenol) measured in this work: (Δ) 523 K, (\square) 573 K. Calculated values with the PC-SAFT equation of state: (.....) $k_{ij} = 0$, (–) $k_{ij} = 0.057$. Pure component vapor pressures measured in this work marked red.

model compared to the predicted one. It was also observed from the decreased values of the average absolute and relative deviations with the binary interaction parameter regression in Table 8.

3.2.3. Non-random Two-Liquid activity coefficient model

The non-random two-liquid (NRTL) activity coefficient model developed by Renon and Prausnitz [14] is based on the local composition theory of Wilson [28] and the two-liquid solution theory of Scott [29]. The NRTL model contains three adjustable parameters that are specific for each binary system [14]. These adjustable parameters are τ_{ij} or $(g_{ij} - g_{jj})/RT$, τ_{ji} or $(g_{ji} - g_{ii})/RT$ and α_{ij} . The two energy interaction parameters account for pure-component liquid interactions (g_{ii} and g_{jj}) and mixed-liquid interactions (g_{ij} and g_{ji}). The non-randomness factor (α_{ij}) can be set a priori. In

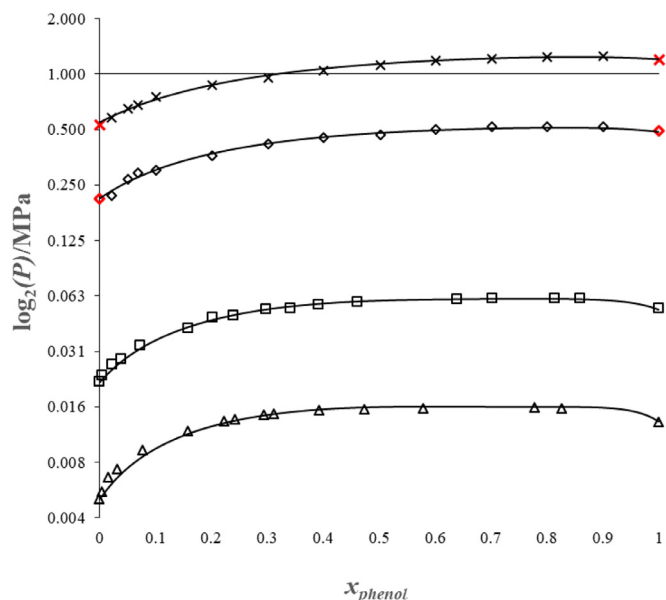


Fig. 7. The bubble point pressures (P) of n -dodecane + phenol system (x_{phenol} – mole fraction of phenol) measured in this work: (\diamond) 523 K, (\times) 573 K. Literature values [31]: (Δ) 393.15 K, (\square) 433.15 K. Calculated values with the NRTL activity coefficient model (—). Pure component vapor pressures measured in this work marked red.

this work, the temperature-dependent energy parameters were regressed, and the non-randomness factor was kept 0.2 as employed in the literature [29]. In regression, NRTL-RK property method was applied. NRTL-RK method uses NRTL activity coefficient model for liquid phase and Redlich-Kwong (RK) equation of state for vapor phase calculation [30]. In this work, the RK binary interaction parameters were not regressed as the highest non-ideality is in liquid phase.

The vapor-liquid criteria are defined as

$$y_i \Phi_i p = x_i \gamma_i \Phi_i^{sat} p_i^{sat} POY \quad (12)$$

where x and y are liquid and vapor mole fractions of component i , ϕ is the vapor phase fugacity, p is the pressure of the system, γ is the activity coefficient, p_i^{sat} is the vapor pressure of the component, POY refers to the Poynting correction and index “sat” refers to the saturated state.

The vapor-liquid equilibrium data for the phenol n -dodecane + phenol was obtained from the literature [31] at the temperature range 393.15–433.15 K. The measured and modeled bubble point pressures of n -dodecane + phenol are shown in Fig. 7. The binary interaction parameters were obtained from the regression of experimental data in this work and the literature data. The absolute and relative pressure deviations and the regressed binary interaction parameters are presented in Table 9. Fig. 7 shows that the experimental data are well fitted with the regressed model for all temperatures.

The measured and modeled bubble point pressures of n -hexadecane + phenol are presented in Fig. 8. Literature data prior to this work were not found for comparison. Fig. 8 indicates that good fit of the experimental data with the regressed model is achieved. The average absolute and relative pressure deviations and the regressed the energy parameters are presented in Table 9.

3.2.4. Regressed parameters

The binary interaction parameters for Peng-Robinson and PC-SAFT equations of state and the regressed NRTL activity coefficient model parameters along with the absolute and relative pressure

Table 9
NRTL parameters for binary mixtures.

component i	Phenol	phenol
component j	n -dodecane	n -hexadecane
Temperature units	K	K
Source	Regressed	Regressed
Property units:		
a_{ij}	-2.45	0.45
a_{ji}	-0.39	-1.31
b_{ij}/K	2138.89	736.89
b_{ji}/K	88.52	375.22
c_{ij}	0.2	0.2
T_{min}/K	393.15	393.15
T_{max}/K	573.15	573.15
$\Delta P_{A,AVG}^a / \text{MPa} \times$	0.0005	-
$\Delta P_{R,AVG}^b / \% \times$	2.55	-
$\Delta P_{A,AVG}^a / \text{MPa}^*$	0.01	0.01
$\Delta P_{R,AVG}^b / \%^*$	1.79	2.37

NRTL binary interaction parameters according to Aspen Plus:

$$\tau_{ij} = a_{ij} + b_{ij}/T, \quad \alpha_{ij} = c_{ij}$$

i and j are providing the order of the components in NRTL model; a - c are the NRTL model parameters; T_{min} and T_{max} are the lowest and the highest temperatures respectively at which parameters are regressed.

\times Literature data [31].

$*$ Data from this work.

a The average absolute pressure deviation $P_{A,AVG} = \frac{(\sum_{i=1}^N |P_{i,meas} - P_{i,calc}|)}{N}$ where N is the number of data points, $P_{i,meas}$ is the measured pressure, $P_{i,calc}$ is the calculated pressure.

b The relative average pressure deviation $P_{R,AVG} = \frac{(\sum_{i=1}^N |(P_{i,meas} - P_{i,calc})/P_{i,meas}|)}{N}$ where N is the number of data points $P_{i,meas}$ is the measured pressure, $P_{i,calc}$ is the calculated pressure.

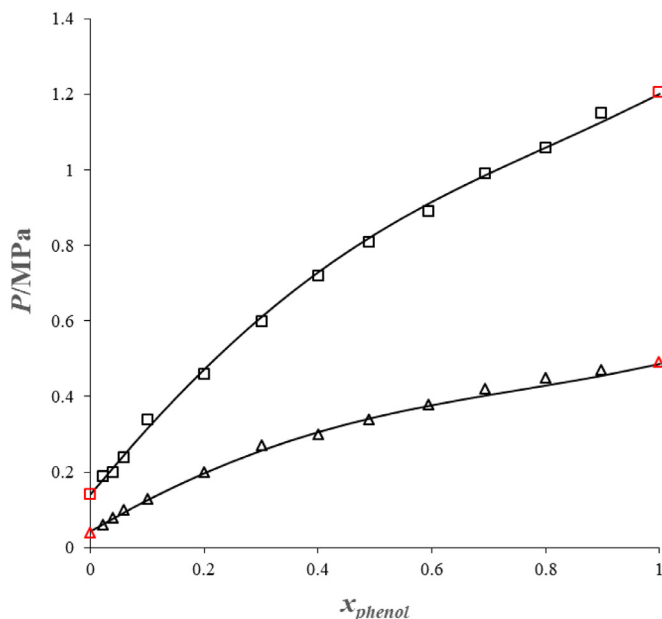


Fig. 8. The bubble point pressures (P) of n -hexadecane + phenol system (x_{phenol} – mole fraction of phenol) measured in this work: (Δ) 523 K, (\square) 573 K. Calculated values with the NRTL activity coefficient model (—). Pure component vapor pressures measured in this work marked red.

deviations between the models and the measured data are presented in Tables 8 and 9, respectively.

3.2.5. VLE phase diagrams

The formation of azeotrope for n -dodecane + phenol was observed from the literature [31] at lower temperatures 393 K and 433K. Similarly, azeotrope formation in this work at 523 K and 573 K confirms that the azeotrope continues at higher temperatures as well. The phase diagrams of n -dodecane + phenol predicted from this work and the literature data [31] are presented in

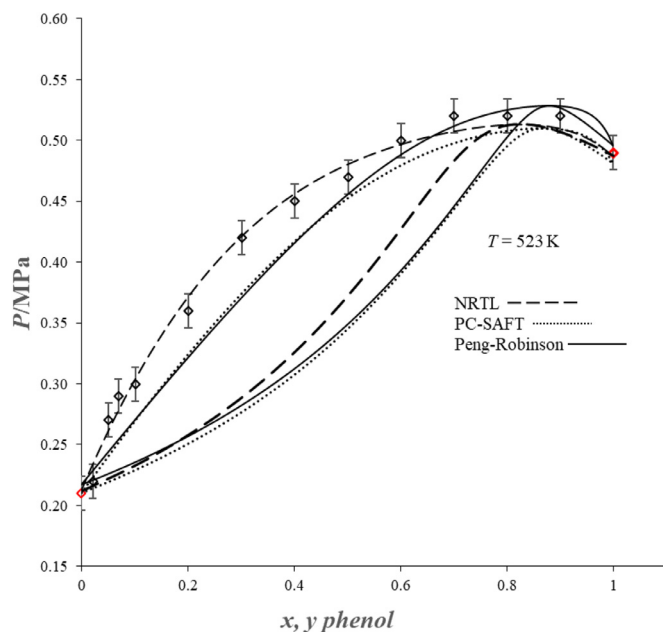


Fig. 9. VLE phase diagram of *n*-dodecane and phenol system measured in this work (\diamond) at 523.15 K. Vapor and liquid phase calculated from the PC-SAFT (.....) $k_{ij} = 0.039$ and Peng-Robinson equations of state (—) $k_{ij} = -0.029$ and, from the regression of NRTL parameters (---). The expanded pressure uncertainty calculated using a coverage factor $k = 2$, $u(P) = 0.01$ MPa used as the error bars.

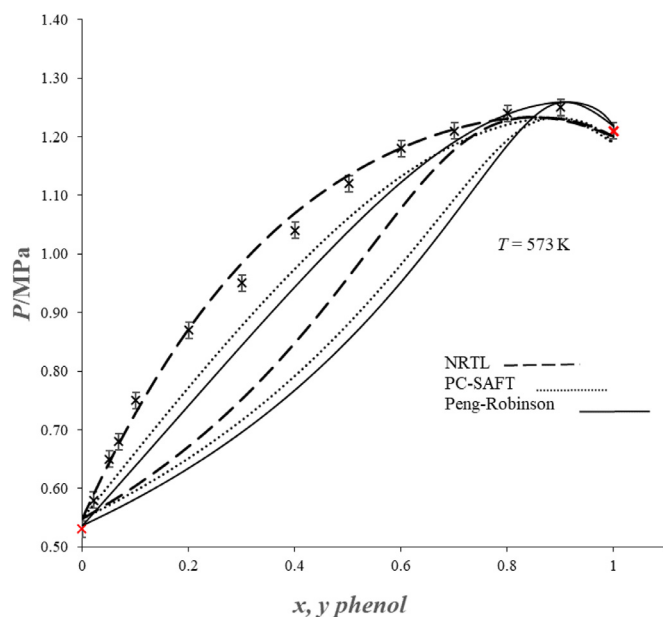


Fig. 10. VLE phase diagram of *n*-dodecane and phenol system measured in this work (\times) at 573.15 K. Vapor and liquid phase calculated from the PC-SAFT (.....) $k_{ij} = 0.039$ and Peng-Robinson equation of state (—) $k_{ij} = -0.029$ and, from the regression of NRTL parameters (---). The expanded pressure uncertainty calculated using a coverage factor $k = 2$, $u(P) = 0.01$ MPa used as the error bars.

Figs. 9–14. The activity coefficient model described the behaviour of the measured and the literature data very well in Figs. 9–11. For the measured data, the NRTL model fit is as good as the data in Figs. 9 and 10. At lower temperatures, the predictions from both the equations of state are in acceptable level in Figs. 12–14. The Peng-Robinson equation of state calculated the azeotropic compositions at higher pressures in comparison to other two models. The optimized azeotropic compositions, temperature and pressures from the models are presented in Table 10.

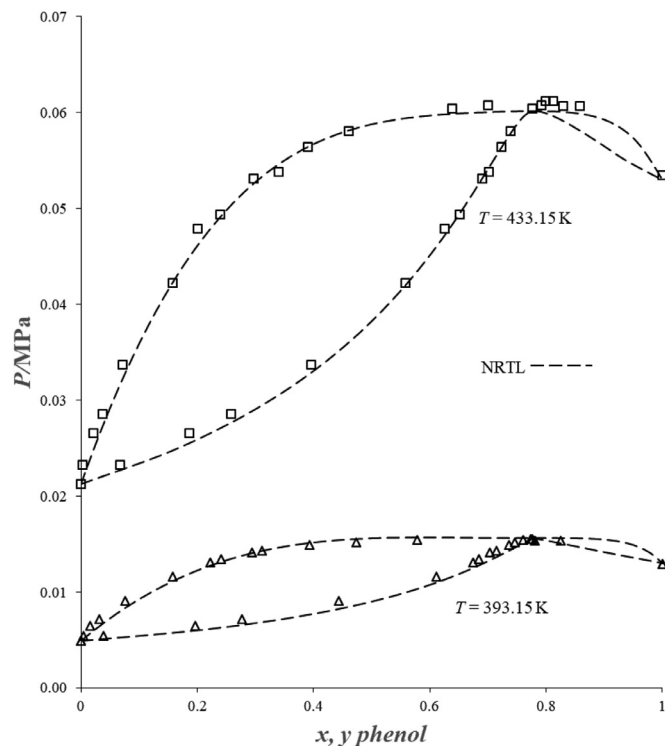


Fig. 11. VLE phase diagram of *n*-dodecane and phenol system obtained from the literature [31] (\square) at 433.15 K and (Δ) at 393.15 K. Vapor and liquid phase calculated from the regression of NRTL parameters.

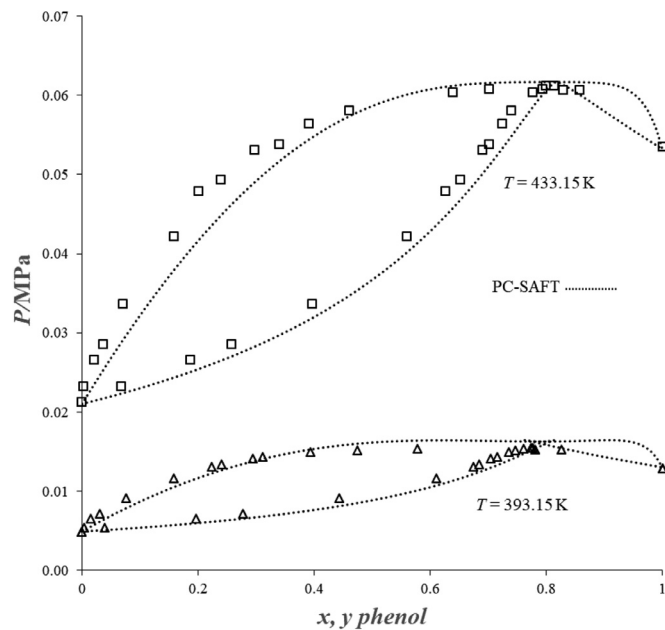


Fig. 12. VLE phase diagram of *n*-dodecane and phenol system obtained from the literature [31] (\square) at 433.15 K and (Δ) at 393.15 K. Vapor and liquid phase calculated from the PC-SAFT equation of state (.....) $k_{ij} = 0.039$.

3.2.6. Azeotropic compositions

The VLE measurement near the azeotropic regions is challenging as a minor experimental error could lead to relatively large shift in azeotropic points. A thermodynamic model regressed over a wide range of compositions is reliable as well in predicting the azeotropic points. Therefore, the azeotropic compositions were calculated using equations of state and activity coefficient model employing the phase equilibrium data.

Table 10

Azeotropic compositions, pressures and temperatures calculated from the PC-SAFT ($k_{ij} = 0.057$) and the Peng-Robinson ($k_{ij} = -0.029$) equation of states and, from the regression of NRTL activity coefficient model for *n*-dodecane + phenol system from this work and the literature data, along with measured the azeotropic compositions from the literature.

	Temperature (K)	Azeotropic composition (x_{phenol})	Azeotropic pressure (MPa)
Peng-Robinson	393.15 ^a	0.804	0.016
	433.15 ^a	0.826	0.062
	523.15 ^b	0.880	0.528
	573.15 ^b	0.909	1.259
PC-SAFT	393.15 ^a	0.792	0.016
	433.15 ^a	0.817	0.062
	523.15 ^b	0.866	0.510
	573.15 ^b	0.888	1.231
NRTL	393.15 ^a	0.771	0.015
	433.15 ^a	0.793	0.060
	523.15 ^b	0.826	0.509
	573.15 ^b	0.853	1.239
Literature [31]	393.15	0.7810	0.0155
	433.15	0.8020	0.0612
Literature [32]	450.85	0.778	0.10132
Literature [33]	450.73	0.7900	0.10133

Estimated uncertainty in T , P , x_{phenol} are respectively, $u(T) = 0.003$ K, $u(P) = 20$ Pa, $u(x_{phenol}) = 0.00003$ to 0.00086 for the literature data [31].

Estimated uncertainty in T , P , x_{phenol} are respectively, $u(T) = 0.12$ K, $u(P) = 0.01$ MPa, $u(x_{phenol}) = 0.0001$ to 0.008 in this work.

^a Calculated from the literature data [31].

^b Calculated from this work.

The literature [31] and the calculated azeotropic compositions for *n*-dodecane and phenol along with azeotropic temperatures and pressures are presented in Table 10. The calculated azeotropic compositions x_{az} at azeotropic pressures are plotted as a function of temperature in Fig. 15, together with azeotropic data determined by other authors [32,33]. Fig. 15 shows the temperature dependence of the azeotropic points. The Peng-Robinson equation of state predicted the azeotropic compositions with higher phenol concentration in comparison to PC-SAFT and NRTL model. Moreover, the azeotropic compositions calculated from the NRTL model correlate well with the literature data in Fig. 15.

4. Discussions

4.1. PC-SAFT parameters for phenol

The phenol PC-SAFT parameters with 2B association scheme were obtained from different sources [8,22,34]. These pure-component PC-SAFT parameters were evaluated against the pure-component vapor pressure and the molar volume data retrieved with the Aspen Plus from the NIST ThermoData Engine database. The average absolute vapor pressure and molar volume deviations for phenol using PC-SAFT parameters from various sources are presented in Table 11. The PC-SAFT parameters for phenol available in Aspen Plus resulted in the lowest vapor pressure deviations presented in Table 11. Therefore, the pure-component PC-SAFT parameters for phenol available in Aspen Plus were employed for modeling in this work.

4.2. Vapor pressures predictions

The experimental pure components vapor pressures are in good agreement with the vapor pressures predicted from the Peng-Robinson equation of state for all the temperatures 393 K–573 K in Figs. 3,4,9,10,13 and 14. Similarly, the pure components vapor pressures predicted from the PC-SAFT equation of state agree well with the experimental data at temperatures 393–523 K in Figs. 6,9 and 13. However, at 573 K the experimental phenol vapor pres-

Table 11

Average absolute vapor pressure and molar volume deviations of phenol obtained with PC-SAFT equation of state parameters from various sources. Experimental data are taken from NIST ThermoData Engine database.

References	[8]	[23]	[34] ^e
m_i ^a	4.2473	2.6844	3.78605
σ_i ^a / Å	3.0341	3.5660	3.2007
ϵ_i/k^a / K	281.12	250.37	293.649
k^{AIBi} ^a	1.63×10^{-7}	0.086578	0.00634
ϵ^{AIBi}/k^a / K	4300	2827.6	1640.63
$\Delta P_{vap,A,AVG}$ ^b / MPa	0.003	0.03	0.001
$\Delta v_{i,A,AVG}$ ^c / cm ³ mol ⁻¹	1.82	0.2	0.53
T_{range} ^d / K	343–585	343–585	343–585

^a PC-SAFT parameters: the segment number m_i , the segment diameter σ_i , the segment energy ϵ_i/k , the effective association volume k^{AIBi} , the association energy ϵ^{AIBi}/k .

^b Pure component average absolute vapor pressure deviation using PC-SAFT parameters: $\Delta P_{vap,A,AVG} = \frac{(\sum_{i=1}^N |P_{i,lit} - P_{i,calc}|)}{N}$ where $N = 54$ is the number of data points, $P_{i,lit}$ is the vapor pressure (Pa) value from the literature, $P_{i,calc}$ is the calculated vapor pressure (Pa).

^c Pure component average absolute molar volume deviation using PC-SAFT parameters: $\Delta v_{i,A,AVG} = \frac{(\sum_{i=1}^N |v_{i,lit} - v_{i,calc}|)}{N}$ where $N = 95$ is the number of data points, $v_{i,lit}$ is the molar volume (cm³ mol⁻¹) value from the literature, $v_{i,calc}$ is the calculated molar volume (cm³ mol⁻¹).

^d Temperature range that was used in the regression of PC-SAFT parameters.

^e Pure component PC-SAFT parameters available in Aspen Plus [34] obtained from NIST-TRC databank.

sure deviates from the PC-SAFT regressed model in Figs. 6 and 10. As presented in Table 5, the comparison of measured vapor pressures of phenol in this work with the literature value showed reliable results as the deviations are within the correlation and the experimental uncertainties. It shows that the vapor pressures prediction would probably improve with the temperature-dependent pure component PC-SAFT parameters for phenol at higher temperatures.

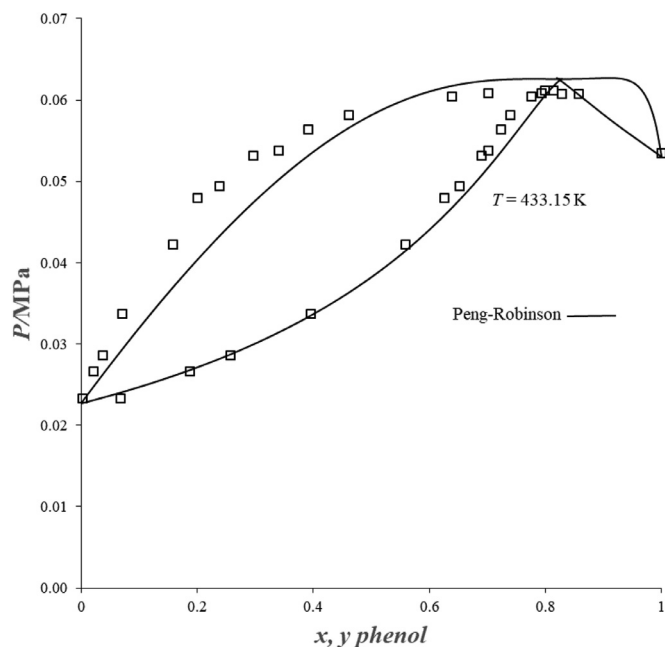


Fig. 13. VLE phase diagram of *n*-dodecane + phenol system from the literature [31] at (□) 433.15 K. Vapor and liquid phase calculated from the Peng-Robinson equation of state (—) $k_{ij} = -0.029$.

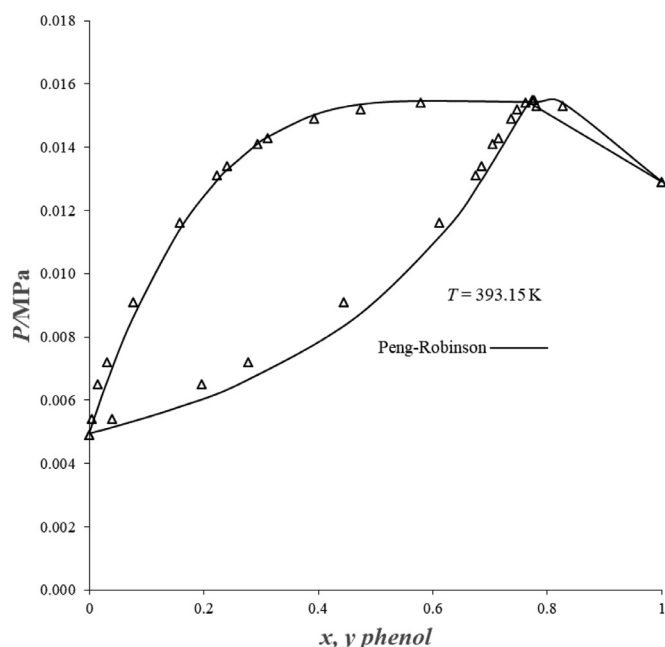


Fig. 14. VLE phase diagram of *n*-dodecane + phenol system from the literature [31] at (Δ) 393.15 K. Vapor and liquid phase calculated from the Peng-Robinson equation of state (—) $k_{ij} = -0.029$.

4.3. Isobaric VLE

The isobaric phase diagram at 101.32 kPa for *n*-dodecane + phenol was calculated using the Peng-Robinson and PC-SAFT equations of state and the NRTL model, presented in Fig. 16 with the measurements from the literature [32]. The regressed parameters presented in Tables 8 and 9 were employed for the phase diagram calculation. The literature data and the calculated phase diagram are presented in Fig. 16. Fig. 16 illustrates that the liquid phase and the azeotropic points predicted from the NRTL model are in good agreement with the experimental data.

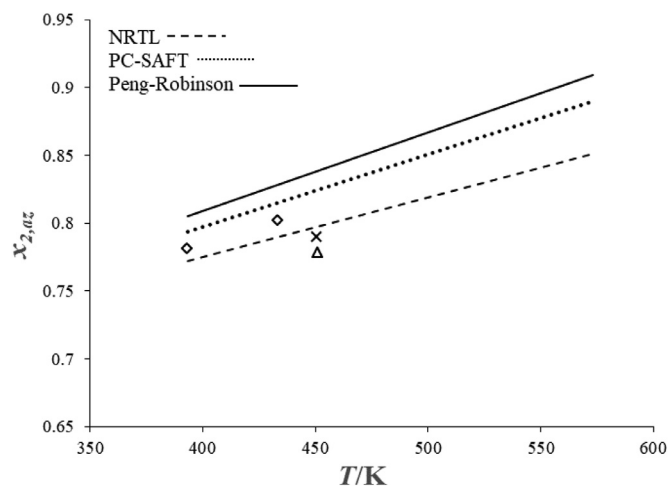


Fig. 15. Azeotropic compositions for *n*-dodecane (1) + phenol (2) system calculated from the Peng-Robinson (—) and PC-SAFT (....) equations of state and the NRTL model (---). Azeotropic data from literature; (◇) 393 K and 433 K [31], (Δ) 450.85 K [32], (x) 450.73 K [33].

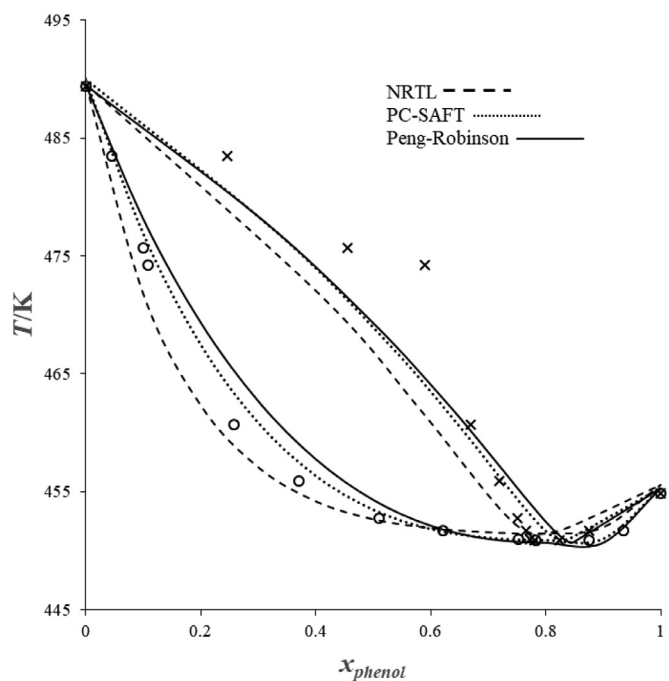


Fig. 16. Isobaric VLE phase diagram calculated from the NRTL model, the PC-SAFT and the Peng-Robinson equations of state. The measured liquid (o) and vapor phase (x) from the literature [32].

This good predictive ability of the NRTL model was also observed for the isothermal VLE data as described in Section 3.2.3.

5. Conclusions

The phase behaviour of pyrolysis oil components is required to improve the thermodynamic models and for the analysis of distillation and other vapor-liquid separation processes. The phase equilibrium is challenging to measure at elevated temperature, especially for the highly flammable and toxic chemical compounds. In addition, accuracy of experimental data is particularly dependent on the measurement methods and the measuring units. This paper presents the bubble point pressures measured at 523 K and 573 K for hydrocarbons and phenol systems using a continuous flow apparatus. The bubble point formation indicated a phase transi-

tion, which was visually observed from the video recording. The pure component vapor pressures of water, phenol, *n*-dodecane and *n*-hexadecane were measured in order to illustrate the measurement accuracy of the measuring apparatus and the method. The measured vapor pressures of the pure components were compared with the literature correlation. The vapor pressure deviations were within the uncertainty of the measurements.

Bubble point pressures of *n*-dodecane + phenol and *n*-hexadecane + phenol were measured at 523 K and 573 K. The measured bubble points can be used for the phase behaviour study of model components and to help design the pyrolysis oil separation process. The measured systems were modeled with Peng-Robinson and PC-SAFT equations of state and, NRTL activity coefficient model. The binary interaction parameters of Peng-Robinson, PC-SAFT and NRTL models were optimized. The NRTL activity coefficient model predicted the behaviour of the measured systems and the literature data very well covering the temperature range 393 K–573 K. In this work, the Peng-Robinson equation of state has proven good predictive capacity to represent hydrocarbons and phenol (oxygenate) with only one parameter regression. Additionally, the PC-SAFT equation of state predicted the measured systems very well with one binary interaction parameter fit. As a result, both equations of state and the activity coefficient model can be applied as the thermodynamic models for the measured systems. The temperature-dependent pure component PC-SAFT parameters could possibly improve the vapor pressure prediction for elevated temperatures. In this phase equilibrium study, the *n*-dodecane + phenol system showed azeotropic behaviour.

Credit author statement

Roshi Dahal measured the bubble point pressures of the pure components and mixtures. Roshi Dahal modeled the measured system, wrote the draft, managed the corrections of the collaborators as well as the reviewers' comments and wrote the response letter. Juha-Pekka Pokki guided in the modeling part. Petri Uusi-Kyyny and Ville Alopaeus evaluated the work, listed important remarks that should be discussed in the manuscript and took role in improving the clarity and readability of the text.

Declaration of Competing Interest

The authors declare that they have no known competing financial interests or personal relationships that could have appeared to influence the work reported in this paper.

Acknowledgements

Roshi Dahal acknowledges Fortum and Neste Foundation for the financial support. Many thanks to Dr. Pia Lappalainen for reading and providing suggestions for language improvement.

References

- [1] A.V. Bridgwater, Review of fast pyrolysis of biomass and product upgrading, *Biomass Bioenergy* (2012), doi:10.1016/j.biombioe.2011.01.048.
- [2] A.R. Rahimi, J.M. García, Chemical recycling of waste plastics for new materials production, *Nature Rev. Chem.* (2017), doi:10.1038/s41570-017-0046.
- [3] M.S. Qureshi, et al., Pyrolysis of plastic waste: Opportunities and challenges, *J. Anal. Appl. Pyrolysis* (2020), doi:10.1016/j.jaap.2020.104804.
- [4] J. Hopewell, R. Dvorak, E. Kosior, Plastics recycling: Challenges and opportunities, *Philos. Trans. R. Soc. B: Biol. Sci.* (2009), doi:10.1098/rstb.2008.0311.
- [5] B.K. Sharma, B.R. Moser, K.E. Vermillion, K.M. Doll, N. Rajagopalan, Production, characterization and fuel properties of alternative diesel fuel from pyrolysis of waste plastic grocery bags, *Fuel Process. Technol.* (2014), doi:10.1016/j.fuproc.2014.01.019.

- [6] H. Hassan, J.K. Lim, B.H. Hameed, Recent progress on biomass co-pyrolysis conversion into high-quality bio-oil, *Bioresour. Technol.* (2016), doi:10.1016/j.biortech.2016.09.026.
- [7] A. Oasmaa, S. Czernik, Fuel oil quality of biomass pyrolysis oils - state of the art for the end users, *Energy Fuels* (1999), doi:10.1021/ef980272b.
- [8] D. Nguyenhuynh, S.T.K. Tran, C.T.Q. Mai, Predicting the Phase Behavior of Alcohols, Aromatic Alcohols, and Their Mixtures Using the Modified Group-Contribution Perturbed-Chain Statistical Associating Fluid Theory, *Ind. Eng. Chem. Res.* (2019), doi:10.1021/acs.iecr.9b03198.
- [9] D. C. Elliott, "Historical developments in hydroprocessing bio-oils," *Energy and Fuels*. 2007, doi: 10.1021/ef070044u.
- [10] S.H. Jung, M.H. Cho, B.S. Kang, J.S. Kim, Pyrolysis of a fraction of waste polypropylene and polyethylene for the recovery of BTX aromatics using a fluidized bed reactor, *Fuel Process. Technol.* (2010), doi:10.1016/j.fuproc.2009.10.009.
- [11] P.T. Williams, E.A. Williams, Fluidised bed pyrolysis of low density polyethylene to produce petrochemical feedstock, *J. Anal. Appl. Pyrolysis* (1999), doi:10.1016/S0165-2370(99)00011-X.
- [12] D.Y. Peng, D.B. Robinson, A New Two-Constant Equation of State, *Ind. Eng. Chem. Fundam.* (1976), doi:10.1021/i160057a011.
- [13] J. Gross, G. Sadowski, Application of the perturbed-chain SAFT equation of state to associating systems, *Ind. Eng. Chem. Res.* (2002), doi:10.1021/ie010954d.
- [14] H. Renon, J.M. Prausnitz, Local compositions in thermodynamic excess functions for liquid mixtures, *AIChE J.* (1968), doi:10.1002/aic.690140124.
- [15] P. Uusi-Kyyny, M.S. Qureshi, J.P. Pokki, V. Alopaeus, D. Richon, 110th Anniversary: Critical Properties and High Temperature Vapor Pressures for Furan, 2-Methylfuran, 2-Methoxy-2-methylpropane, 2-Ethoxy-2-methylbutane, *n*-Hexane, and Ethanol and Bubble Points of Mixtures with a New Apparatus, *Ind. Eng. Chem. Res.* (2019), doi:10.1021/acs.iecr.9b02912.
- [16] D. I., for P. P. S. by AIChE and D. I. for P. P. S. by AIChE, *DIPPR Project 801, 2005 - Full Version*.
- [17] Group 1 of the Joint Committee for Guides in Metrology (JCGM/WG1) Evaluation of measurement data - Guide to the expression of uncertainty in measurement, *Int. Organ. Stand. Geneva ISBN*, 2008, doi:10.1373/clinchem.2003.030528.
- [18] R. P. Daubert, T. E. Danner, "Physical and Thermodynamic Properties of Pure Compounds: Data Compilation Title," Taylor Fr. Washing. D.C., 1998.
- [19] B.E. Poling, J.M. Prausnitz, J.P. O'Connell, *The Properties of Gases & Liquids - Fifth Edition*, 2001.
- [20] J.C. Bloxham, M.E. Redd, N.F. Giles, T.A. Knotts, W.V. Wilding, Proper Use of the DIPPR 801 Database for Creation of Models, Methods, and Processes, 2020, doi:10.1021/acs.jced.0c00641.
- [21] W. Wagner, A. Prueß, The IAPWS formulation 1995 for the thermodynamic properties of ordinary water substance for general and scientific use, *J. Phys. Chem. Ref. Data* (2002), doi:10.1063/1.1461829.
- [22] J. Gross, G. Sadowski, Perturbed-chain SAFT: An equation of state based on a perturbation theory for chain molecules, *Ind. Eng. Chem. Res.* (2001), doi:10.1021/ie0003887.
- [23] I.V. Prikhod'ko, F. Tumakaka, G. Sadowski, Application of the PC-SAFT equation of state to modeling of solid-liquid equilibria in systems with organic components forming chemical compounds, *Russ. J. Appl. Chem.* (2007), doi:10.1134/S1070427207040040.
- [24] M. Saajanlehto, P. Uusi-Kyyny, P. Haimi, M. Pakkanen, V. Alopaeus, A novel continuous flow apparatus with a video camera system for high pressure phase equilibrium measurements, *Fluid Phase Equilib.* (2013), doi:10.1016/j.fluid.2013.07.001.
- [25] J.A. Barker, Determination of activity coefficients from total pressure measurements, *Aust. J. Chem.* (1953), doi:10.1071/CH9530207.
- [26] W.G. Chapman, G. Jackson, K.E. Gubbins, Phase equilibria of associating fluids, *Mol. Phys.* (1988), doi:10.1080/00268978800101601.
- [27] S.H. Huang, M. Radosz, Equation of State for Small, Large, Polydisperse, and Associating Molecules, *Ind. Eng. Chem. Res.* (1990), doi:10.1021/ie00107a014.
- [28] G.M. Wilson, Vapor-Liquid Equilibrium. XI. A New Expression for the Excess Free Energy of Mixing, *J. Am. Chem. Soc.* (1964), doi:10.1021/ja01056a002.
- [29] G. Scatchard, S.E. Wood, J.M. Mochel, Vapor-Liquid Equilibrium. VII. Carbon Tetrachloride-Methanol Mixtures, *J. Am. Chem. Soc.* (1946), doi:10.1021/ja01214a025.
- [30] O. Redlich, J.N.S. Kwong, On the thermodynamics of solutions. V. An equation of state. Fugacities of gaseous solutions, *Chem. Rev.* (1949), doi:10.1021/cr60137a013.
- [31] J. Schmelzer, H. Niederbroeker, S. Partzsch, R. Voekler, R. Meinhardt, in: *EL-DATA: The International Electronic Journal of Physico-Chemical Data*, 2, 1996, pp. 153–162.
- [32] A.Ya. Aarna, T.K.Tr Kaps, Equilibrium between the liquid and the vapor in binary mixtures monohydric phenols + hydrocarbons, *Tallin. Politekh. Inst.* 285 (1970) 3.
- [33] J. Gmehling, J. Menke, J. Krafczyk, K Fischer, *Azeotropic Data, Part 1, 11nd edition*, WILEY-VCH, 2004.
- [34] Aspen Technology Inc. Aspen Plus, 2011.